Finite-lens effect on self-lensing in detached white dwarfs-main sequence binary systems

Sajadian, S.; Fatheddin, H.

The Astronomical Journal, 169:3 (11pp), 2025 January https://doi.org/10.3847/1538-3881/ad81d1

Finite-lens Effect on Self-lensing in Detached White Dwarfs-main Sequence Binary Systems

Sedighe Sajadian[1] and Hossein Fatheddin[2]
[1] Department of Physics, Isfahan University of Technology, Isfahan 84156-83111, Iran; s.sajadian@iut.ac.ir
[2] Leiden Observatory, Leiden University, P.O. Box 9513, NL-2300 RA Leiden, The Netherlands
Received 2024 August 28; revised 2024 September 25; accepted 2024 September 25; published 2024 December 3

Abstract

In edge-on and detached binary systems, including a white dwarf (WD) and a main-sequence (MS) star system (or WDMS), when the source star is passing behind the compact companion its light is bent and magnified. Meanwhile, some part of its image's area is obscured by the WD's disk. These two effects occur simultaneously, and the observer receives the stellar light magnified and partially obscured due to the finite lens size. We study these effects in different WDMS binary systems numerically using inverse ray-shooting and analytically using approximate relations close to reality. For WDMS systems with long orbital periods $\gtrsim$300 days and $M_{\rm WD} \gtrsim 0.2M_{\odot}$ (where $M_{\rm WD}$ is the mass of the WD), lensing effects dominate the occultations due to finite-lens effects, and for massive WDs with masses higher than solar mass, no occultation happens. The occultations dominate self-lensing signals in systems with low-mass WDs ($M_{\rm WD} \lesssim 0.2M_{\odot}$) in close orbits with short orbital periods $T \lesssim 50$ days. The occultation and self-lensing cancel each other out when the WD's radius equals $\sqrt{2}$ times the Einstein radius, regardless of the source radius, which offers a decreasing relation between the orbital period and WD mass. We evaluate the errors in the maximum deviation in the self-lensing/occultation normalized flux, which is done by using its known analytical relation, and conclude that these errors could be up to 0.002, 0.08, and 0.03 when the orbital period is $T = 30$, 100, and 300 days, respectively. The size of stellar companions in WDMS systems has a twofold manner, decreasing the depth of self-lensing/occultation signals but enlarging their width.

Unified Astronomy Thesaurus concepts: Astronomical simulations (1857); Eclipsing binary stars (444); Compact binary stars (283); Gravitational lensing (670); Occultation (1148); White dwarf stars (1799); Computational methods (1965)

1. Introduction

Gravitational lensing refers to the bending of light due to passing through the gravitational field of a massive object (see, e.g., J. Soldner 1921). The correct amount of the deflection angle in a lensing event was derived from the general theory of relativity (e.g., E. E. Clark 1972; J. Renn et al. 1997). Several kinds of gravitational lensing exist depending on the lens mass, the impact parameter, and the distances between the lens, source object, and observer (P. Schneider et al. 1992; R. Narayan & M. Bartelmann 1996). The first kind is gravitational microlensing, which refers to a temporary enhancement in the brightness of a background star that is collinear with a foreground and massive object (A. Einstein 1936; S. Liebes 1964; S. Refsdal & H. Bondi 1964). This kind of lensing can be utilized as a method for discovering and characterizing isolated and even dark objects, ranging from extrasolar planets to isolated stellar-mass black holes in our galaxy (see, e.g., B. S. Gaudi 2012; S. Sajadian 2021; K. C. Sahu et al. 2022). In cosmological scales, either weak or strong lensing happens by generating giant arcs or multiple images from a distant and bright source galaxy. One of the most important applications of these kinds of lensing in cosmological scales is measuring the Hubble constant and studying its variations with the cosmological redshift and the Hubble tension (see, e.g., A. G. Riess et al. 1998, 2024).

Gravitational self-lensing is another type of lensing which occurs in detached and edge-on binary systems containing main-sequence (MS) stars and compact objects (e.g., A. Gould 1995). In such systems, whenever the companion star is passing behind the compact object as seen by the observer, its light is bent and magnified due to passing through the gravitational field of the compact object. Self-lensing is a method to detect and characterize compact objects in *detached* binary systems with MS stars. Up to now, five self-lensing events have been discovered from Kepler data, all of which were related to binary systems including white dwarfs (WDs) and MS stars (otherwise known as WDMS systems; E. Kruse & E. Agol 2014; H. Kawahara et al. 2018; K. Masuda et al. 2019). Recently, N. Yamaguchi et al. (2024) revisited the last self-lensing target (KIC 8145411) using high-resolution imaging, and found that it was a triplet system including two solar-type stars and one WD with a mass of $\sim 0.53M_{\odot}$. Therefore, all five discovered self-lensing events were due to WDs more massive than $0.5M_{\odot}$ in wide orbits with orbital periods of $T \in [88, 728]$ days. Additionally, another self-lensing event (first discovered from Kepler data) was recovered by the Transiting Exoplanet Survey Satellite (TESS; G. R. Ricker et al. 2014) telescope and reported in N. M. Sorabella et al. (2024).[3] With regards to the possibility of detecting compact objects through self-lensing/eclipsing signals in TESS data, S. Sajadian & N. Afshordi (2024) performed comprehensive simulations, and predicted that 15–18 WDs and 6–7 neutron stars would be discovered from the TESS Candidate Target List.

[3] https://science.nasa.gov/mission/tess/

To correctly extract the physical parameters of compact objects in self-lensing events, studying their light curves is a crucial step. In self-lensing events, the lens objects and source stars are close to each other, and accordingly their Einstein radii are small in comparison to those in common microlensing events toward the Galactic bulge. The Einstein radius is the radius of the image's ring when the observer, source star, and lens object are completely aligned. For instance, in a WDMS binary system whose orbital radius is 1 au, the Einstein radius is $\simeq$0.02–0.05$R_{\odot}$, whereas for common microlensing events toward the Galactic bulge, it is $R_{\rm E} \sim$ 1–2 au. Lensing events with small Einstein radii are affected by (i) the finite-source effect (H. J. Witt & S. Mao 1994), because their source radii (projected on the lens plane and normalized to the Einstein radius) are considerable $\rho_{\star} = R_{\star,{\rm p}}/R_{\rm E} \gtrsim 1$, and (ii) the finite-lens effect (see, e.g., C. Han 2016). Here, $R_{\star,{\rm p}} = R_{\star}\, D_{\rm l}/(D_{\rm l} - x_{\rm o})$ is the source radius ($R_{\star}$) which is projected on the lens plane, $D_{\rm l}$ is the compact object's distance from the observer, and $x_{\rm o}$ is the radial distance of the companion star from the compact object in the line of sight. The second effect occurs when the size of the lens object is comparable to the Einstein radius that could cover some part of the image's disk. Among different compact objects, WDs have the largest radii, with an order of magnitude similar to the Einstein radii in self-lensing events.

Several papers have introduced, studied, and evaluated self-lensing signals in binary systems (A. Maeder 1973; A. Gould 1995; E. Agol 2002; C. Han 2016). In this work, we extend this research and numerically/analytically study some other properties of self-lensing signals affected by finite-lens effects in WDMS binary systems. Here, we will (i) examine in what systems occultations due to finite-lens effects are either dominant or negligible in comparison with the self-lensing signals; (ii) evaluate maximum deviations due to occultation, and self-lensing/occultation effects in stellar light curves from different WDMS binary systems; (iii) estimate the errors due to modeling self-lensing peaks using the known analytical relations; and (iv) discuss the widths of the self-lensing/occultation signals.

The paper is organized as follows. In Section 2, we first introduce our formalism for generating self-lensing signals and finite-lens effects in detached and edge-on WDMS binary systems. Then, in Section 2.2, we generate the stellar images formed during a self-lensing event and evaluate what WDMS systems have dominant/negligible occultations (in comparison with self-lensing signals). In Section 3, we simulate and study the properties of self-lensing/occultation stellar light curves. In Sections 3.1–3.3, we evaluate the maximum deviations in these stellar light curves based on analytical relations, the accuracy of the known analytical relations to derive peaks of self-lensing/occultation signals based on the inverse ray-shooting (IRS) method, and the widths of the self-lensing/occultation signals, respectively. In Section 4, we review the key points and conclusions.

2. Self-lensing and Finite-lens Effects

A. Maeder (1973) first introduced the lensing effect in different binary systems and concluded that the lensing amplitudes in binary systems containing two compact objects would be 10–25 times larger than those in binary systems including at least one MS star. The probabilities (lensing optical depths) of the self-lensing signals which occur in binary systems containing one or two compact objects were estimated by A. Gould (1995). The analytical and approximate relations for magnification factors during self-lensing events offered by A. Maeder (1973) were extended to nonuniform source stars with a limb-darkening brightness profile by E. Agol (2002). Recently, C. Han (2016) reported a continuous degeneracy while modeling self-lensing/occultation signals that prevents us from uniquely inferring the mass of compact objects. We here extend this research, and study other points.

In this section, we first introduce our formalism to calculate self-lensing and occultation effects. We then compare the occultation and magnification effects in different WDMS binary systems and determine in what systems the occultation effects dominate self-lensing signals and vice versa.

2.1. Formalism

Our formalism to simulate a detached binary system containing a MS star and a WD that are rotating around their common center of mass was first described in detail in S. Sajadian & N. Afshordi (2024), and here we review it only briefly. To simulate a WDMS binary system, we consider the following parameters: $M_{\star}$, the mass of the MS star; $R_{\star}$, the radius of the MS star; $M_{\rm WD}$, the mass of the WD; and $R_{\rm WD}$, the radius of the compact object. We also assume the period and eccentricity of their orbits are T and ϵ, respectively.

If there is no external force and the binary system is isolated, (i) their center of mass is either moving with a constant speed or fixed, and (ii) one component is moving over an ellipse with the same orbital period T concerning the second component. The semimajor axis a of this ellipse can be determined by Kepler's third law.

There are two coordinate systems: (i) the orbital coordinate system (x, y, z), where z is normal to the orbital plane, and (x, y) are on the orbital plane and denote the directions of the major and minor axes, respectively; and (ii) the observer coordinate system ($x_{\rm o}$, $y_{\rm o}$, $z_{\rm o}$), where $x_{\rm o}$ is toward the observer, and ($y_{\rm o}$, $z_{\rm o}$) are on the sky plane and denote the right and up directions, respectively. To convert the first coordinate system to the second one, we need two projection angles: (i) θ, the angle between the semiminor axis and the sky plane (it is not necessary for circular orbits), and (ii) i, the angle between the orbital plane and the line of sight toward the observer, which is the so-called inclination angle. Accordingly, the three components of the position vector of the star with respect to its compact companion in the observer coordinate system are as follows:

$$\begin{aligned} x_{\rm o} &= \cos i\,(-y\sin\theta + x\cos\theta),\\ y_{\rm o} &= y\cos\theta + x\sin\theta,\\ z_{\rm o} &= -\sin i\,(-y\sin\theta + x\cos\theta), \end{aligned} \tag{1}$$

where $x = a(\cos\xi - \epsilon)$ and $y = a\sin\xi\sqrt{1-\epsilon^2}$ describe the stellar position over its orbit in any given time. Here, ξ is the eccentric anomaly and is determined using Kepler's equation (see, e.g., M. Dominik 1998; S. Sajadian & M. Hundertmark 2017).

To simulate a self-lensing signal, we assume that the orbital plane of the binary system is edge-on as seen by the observer, i.e., the inclination angle is small. For an edge-on orbit, when the source star is passing behind the compact object its light is crossing the gravitational field of the compact object and is bent. By comparing the angular positions of the image (ϑ) and the source star (β) in the lens plane, one can reach the raw form

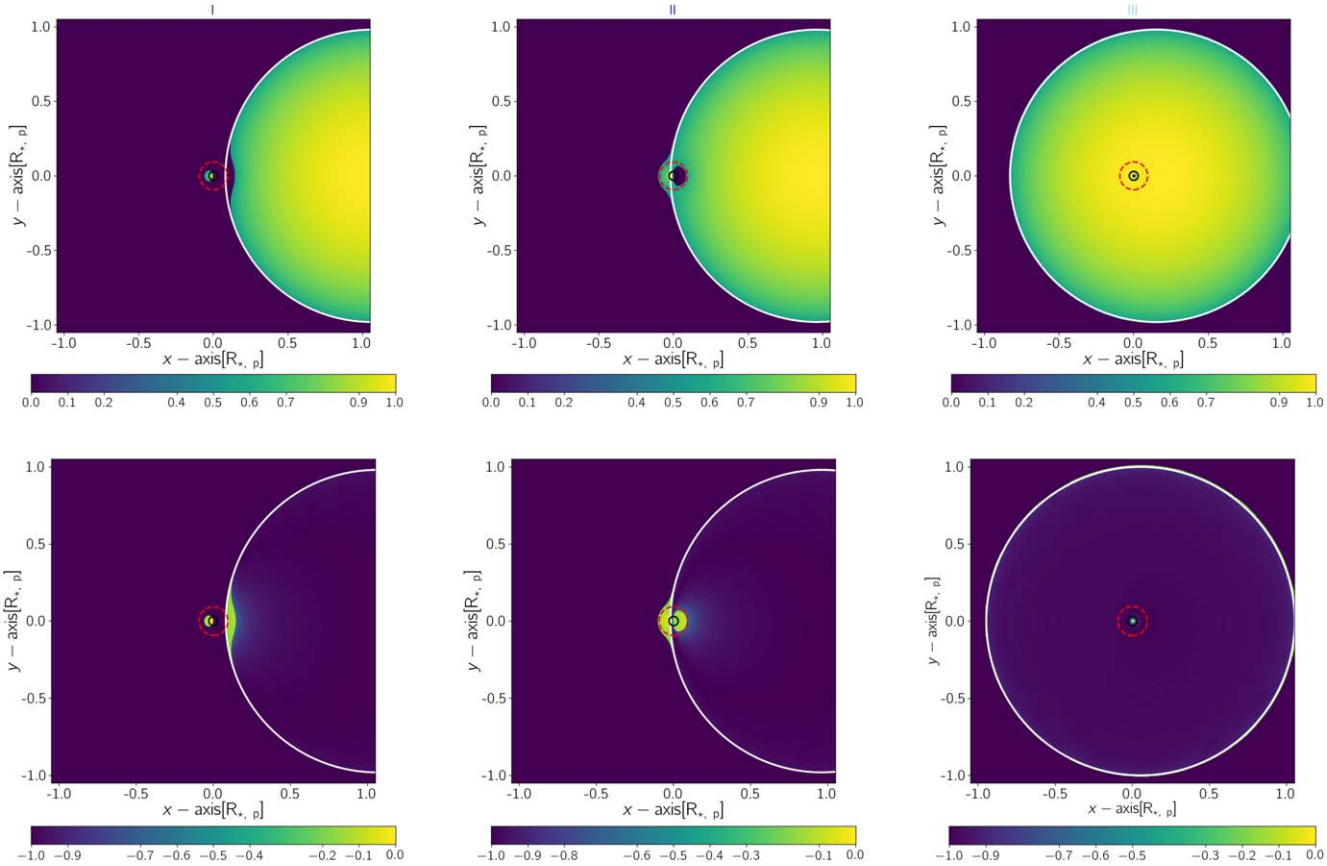

Figure 1. The three top panels show the images formed during the self-lensing of a MS star by its WD companion at three different times. Three bottom panels represent their corresponding residual maps between the projected brightnesses of the images and the source star itself. The white, black, and red (dashed) circles display the edges of the source star, the lens object, and the Einstein radius. The axes are normalized to the source radius projected on the lens plane $R_{\star,\mathrm{p}}$. Two animations from the image maps (https://iutbox.iut.ac.ir/index.php/s/mgoqo9YikR2W2se) and residual maps (https://iutbox.iut.ac.ir/index.php/s/BQ2CC3LfqBbgSpL) while the MS star is passing behind the compact object vs. time are available.

of the lens equation (without any approximation):

$$\tan\beta = \tan\vartheta - [\tan(\alpha - \vartheta) + \tan\vartheta]\frac{D_{\mathrm{ls}}}{D_{\mathrm{s}}}, \qquad (2)$$

where $D_{\mathrm{ls}} = D_{\mathrm{s}} - D_{\mathrm{l}}$, and D_{s} and D_{l} are the source and lens distances from the observer, respectively. In the simulation, D_{l}, the distance of the compact object from the observer, is fixed. In our formalism, $D_{\mathrm{s}} = D_{\mathrm{l}} - x_{\mathrm{o}}$. We note that $\alpha \simeq \frac{4\,G\,M_{\mathrm{WD}}}{c^2\,b}$ is the deflection angle due to the lensing effect, where G is the gravitational constant, c is the speed of light, and $b = \tan\vartheta\, D_{\mathrm{l}}$ is the so-called impact parameter.

Here, we calculate the magnification factor by solving the lens equation (Equation (2)) using the IRS method (R. Kayser et al. 1986; P. Schneider & A. Weiss 1987; J. Wambsganss 1998; S. Sajadian & S. Rahvar 2010). At each given time, we also calculate the fraction of the image's area that is covered by the lens's disk, to evaluate the finite-lens effect.

In our IRS calculations, the size of the lens plane is $5\rho_\star \times 5\rho_\star$, and we divide it into 2500×2500 grids. The position of each grid, $(x_{\mathrm{i}}, y_{\mathrm{i}})$, determines the lensing impact parameter $b = R_{\mathrm{E}}\sqrt{x_{\mathrm{i}}^2 + y_{\mathrm{i}}^2}$, and accordingly $\tan\vartheta = b/D_{\mathrm{l}}$. Using Equation (2), one can indicate the initial line of sight of that light (if it was not bent), i.e., β, and its components, i.e., $(x_\beta, y_\beta) = \eta \times (x_{\mathrm{i}}, y_{\mathrm{i}})/b$, where $\eta = D_{\mathrm{l}}\tan\beta$. Here, we use the fact that the gravitational lens does not change the azimuthal angle of the light. If (x_β, y_β) is one point on the source disk, which is a circle with radius $\rho_\star$ and center $(y_{\mathrm{o}}/R_{\mathrm{E}}, z_{\mathrm{o}}/R_{\mathrm{E}})$, the point $(x_{\mathrm{i}}, y_{\mathrm{i}})$ is over the image's disk. Also, if $b \leqslant R_{\mathrm{WD}}$, we do not receive the light of that part of the image as it is obscured by the lens's disk.

In this formalism, we also consider the linear limb-darkening profile for the surface brightness of the source star as $I = I_0(1 - \Gamma[1 - \mu])$, where I_0 is the brightness at the source's center, Γ is the linear limb-darkening coefficient, $\mu = \sqrt{1 - R^2/R_\star^2}$, and R is the radial distance over the source disk. Based on this explained formalism, we generate the images in self-lensing events and discuss their properties in the next subsection.

2.2. Finite-lens Effect versus Self-lensing

As explained in Section 1, in a self-lensing event the source star and lens object are very close to each other, i.e., $|x_{\mathrm{o}}| \ll D_{\mathrm{l}}$. Hence, in these events the Einstein radius, $R_{\mathrm{E}} = \sqrt{\frac{4\,G\,M_{\mathrm{WD}}}{c^2}\frac{D_{\mathrm{l}}\,|\,x_{\mathrm{o}}\,|}{D_{\mathrm{l}} - x_{\mathrm{o}}}}$, is small ($\sim$0.02–0.05$R_\odot$) in comparison with the Einstein radius of a common microlensing event toward the Galactic bulge (i.e., $\sim$1–2 au). Therefore, in self-lensing events (i) the finite source size is large, $\rho_\star \gtrsim 1$, and (ii) the finite lens size could be significant.

We simulate images of a source star lensed by its compact companion while the source star is passing behind versus time using the IRS method. In the three top panels of Figure 1, we show the images in three different positions of the source star

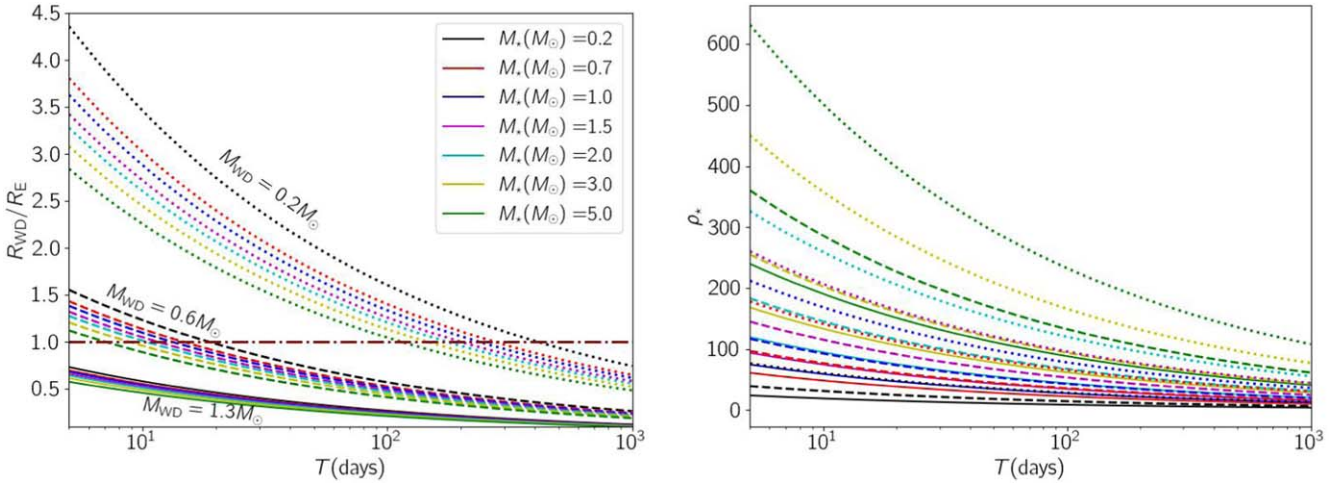

Figure 2. These two plots represent R_{WD}/R_E (left panel) and $\rho_\star$ (right panel) vs. orbital period T (in days) for different detached binary systems including WDs and MS stars. Here, for detached binary systems three different values for the WDs' mass, $M_{WD}(M_\odot) = 0.2$, 0.6, and 1.3 (different line styles), and seven types of MS stars with different masses (different colored curves) are considered. The horizontal dark red line in the left panel shows $R_{WD} = R_E$.

projected on the lens plane. In these figures, the white, black, and red circles specify the source star, lens object, and the Einstein ring, respectively. Accordingly, lensing effects on the source stars are barely noticeable. Hence, in the bottom panels, we show the residual maps (absolute values of the difference between the image maps and the source maps in logarithmic scale). To make these maps we use the following parameters: $M_\star = 0.2M_\odot$, $R_\star = 0.3R_\odot$, $M_{WD} = 1.3M_\odot$, $R_{WD} = 0.002R_\odot$, $T = 60$ days, $i = 0°$, $\theta = 0°$, $\epsilon = 0$, $D_l = 1$ kpc, and $\Gamma = 0.5$.

Accordingly, in lensing events due to a single lens object from a large source star, if the lens is out of the source disk ($u > \rho_\star$) two images are formed. One of them is inside the Einstein radius and very small, and another one is similar to the source star with some deformation at the source's edge. When the lens is over the projected source disk, inside the Einstein ring (the red dashed circles), there exist (i) an empty hole (demagnification) so that its size decreases while the projected distance between the source center and the compact object decrease, and (ii) a lensed part (on the opposite side of that empty hole). Therefore, and according to the three bottom panels, most of the variations during self-lensing happen inside the Einstein radius. If the lens radius is much smaller than the Einstein radius, $R_{WD} \ll R_E$, the finite-lens effect is negligible. But if the lens radius is comparable with the Einstein radius, it will change the overall magnification factor. There is an empty hole in the Einstein radius, and hence the occultation amount depends on the radius of that hole in addition to the R_{WD}, and R_E. We study this point in the next section.

We investigate in what kinds of WDMS binary systems the lens radius has a similar order of magnitude with the Einstein radius or even is larger than it, $R_{WD} \gtrsim R_E$. For WDs, there is a known decreasing relation between their mass and radius as (see, e.g., F. Ambrosino 2020)

$$R_{WD}(R_\odot) = 0.01(M_\odot/M_{WD})^{1/3}. \quad (3)$$

For instance, a typical WD with $M_{WD} \simeq 0.6M_\odot$ has a radius $R_{WD} \simeq 0.012R_\odot$. Using Equation (3), R_{WD}/R_E is given by

$$\frac{R_{WD}}{R_E} \simeq 0.36\,[T(\text{day})]^{2/3}\left(\frac{M_{WD}}{M_\odot}\right)^{5/3}\left[\frac{M_{WD}}{M_\odot} + \frac{M_\star}{M_\odot}\right]^{1/3}. \quad (4)$$

By considering seven types of MS stars and three values for the WDs' mass, we calculate R_{WD}/R_E as shown in the left panel of Figure 2 versus the orbital period T (in days). In Equation (4), we calculate the semimajor axis (for deriving the Einstein radius) using Kepler's third law.

According to this plot, for most WDs and source stars with $M_{WD} \gtrsim 0.2M_\odot$ and $M_\star \in [0.08, 1.2]M_\odot$, if their orbital periods are $T \gtrsim 300$ days (where $R_{WD} \lesssim R_E$ in the left panel of Figure 2) the magnification due to self-lensing dominates the occultation owing to the finite-lens effect. Most massive WDs with $M_{WD} \gtrsim 1.3M_\odot$ (which is close to the Chandrasekhar limit) have very small radii. For these WDs, even considering a wide range of orbital periods $T \in [5, 1000]$ days and different values of $M_\star$, we do not expect a significant finite-lens effect, because they have $R_{WD} \lesssim 0.6R_E$. For common WDs with $M_{WD} \simeq 0.6M_\odot$, if the orbital period is less than $\sim$20 days, their binary systems have $R_{WD} \gtrsim R_E$, i.e., the occultation effect is considerable.

To evaluate the self-lensing signals in these binary systems, in the right panel of Figure 2 we display $\rho_\star$ for the mentioned binary systems versus the orbital period. For WDMS binary systems we can estimate $\rho_\star$ as

$$\rho_\star \simeq 23.4\frac{R_\star(R_\odot)}{\sqrt{M_{WD}(M_\odot)}}\left[\frac{1}{\sqrt{a(\text{au})}} - 2.4\times10^{-9}\frac{\sqrt{a(\text{au})}}{D_l(\text{kp})}\right]. \quad (5)$$

Since the self-lensing signal can be estimated by $1 + 2\rho_\star^{-2}$ (see, e.g., A. Maeder 1973; A. Gould & C. Gaucherel 1996; E. Agol 2003), the smaller the projected and normalized source radii, the larger the self-lensing signals.

According to the two panels of Figure 2, self-lensing signals are dominated by finite-lens effects when R_E is large. Hence, by either increasing the mass of the WD or the orbital period, or both, the self-lensing signal is enhanced and the finite-lens effect is reduced. The highest self-lensing signal happens for most massive WDs ($M_{WD} \sim 1.3M_\odot$) that have dwarf companions in wide orbits. For that reason, all five discovered self-lensing events have $M_{WD} \geqslant 0.5M_\odot$ and $T \geqslant 88$ days (E. Kruse & E. Agol 2014; H. Kawahara et al. 2018; K. Masuda et al. 2019; N. Yamaguchi et al. 2024). For the self-lensing target KIC 8145411, although the initial estimation for the WD mass was $0.2M_\odot$, in conflict with the standard binary evolutionary

path (K. Masuda et al. 2019), later high-resolution photometry data revealed the existence of a third component and indicated the WD mass should in fact be $0.5M_{\odot}$ (N. Yamaguchi et al. 2024).

We note that both $M_{\rm WD}$ and a (which is $\propto T^{2/3}$) have the same effects on $R_{\rm E}$, so that increasing the first one from $0.2M_{\odot}$ to $1.3M_{\odot}$ or increasing the orbital period from 10 to 200 days both reduce $\rho_{\star}$ by a factor of 0.4. Inversely, the occultation effect due to the finite lens size dominates the self-lensing signal when $R_{\rm E}$ is small, which results in large $\rho_{\star}$ and a considerable occultation. We note that both effects (the magnification and occultation) are enhanced when the source radius is reduced. In the next section, we study stellar light curves that contain self-lensing signals affected by the finite-lens effect.

3. Self-lensing/Occultation Light Curves

Using the IRS method, we make a sample of stellar light curves for WDMS binary systems while the source stars are passing behind the compact companions. Some of these light curves are shown in Figure 3. In each panel, the normalized fluxes versus time due to the self-lensing signal, occultation effect, and overlapped self-lensing/occultation effects are shown by green dashed, red dotted–dashed, and black solid curves, respectively. The x-axis is normalized to $t_{\star}$, which is the time of crossing the source radius. The key parameters to generate each of them are given at the top of each panel.

The first panel (Figure 3(a)) represents the light curve due to the WDMS binary system whose lensing-induced images (at three different times, labeled with I, II, and III) are represented in the three top panels of Figure 1. In this light curve, the self-lensing signal is dominant. In the next panel (Figure 3(b)) the occultation effect is dominant. The $R_{\rm E}$ values for these two WDMS binary systems are $0.029R_{\odot}$ and $0.005R_{\odot}$, respectively.

If the enhancements due to the self-lensing and occultation effects have similar orders of magnitude, they cancel each other out. By simulating different stellar light curves from edge-on and detached WDMS binary systems, we find that when $R_{\rm WD} \simeq 1.4R_{\rm E}$, and for any given value of $\rho_{\star}$ in their stellar light curves there are neither self-lensing nor occultation effects. In the next section, we evaluate this point by investigating the maximum deviation in the normalized source flux analytically.

In Figures 3(c) and (d), we display two examples of self-lensing signals that are canceled out by occultation effects. In both cases $R_{\rm WD} \simeq 1.4R_{\rm E}$, whereas they have different values for $\rho_{\star}$. If such stellar light curves are discovered, the equation $R_{\rm WD} \simeq 1.4R_{\rm E}$ will offer a relation between the WD mass and the orbital period (we assume the source star's parameters including its mass are determined from other observations, e.g., spectroscopy). If an eclipsing signal due to transiting the compact object by the source star occurs, it will reveal the orbital period. Accordingly, one can indicate the WD's mass.

In the two last panels (Figures 3(e) and (f)), we represent two more self-lensing events affected by finite-lens effects. In Figure 3(e) the self-lensing signal is higher than the occultation effect, and in the Figure 3(f) the occultation is deeper than the self-lensing signal.

The stellar light curves shown in Figure 3 have similar shapes. Several observing parameters can be extracted from these which are functions of the physical parameters of the source stars and compact objects. For each light curve, these observing parameters are (i) the peak value, (ii) the width, (iii) the deviation from a top-hat model, and (iv) the time of the maximum time derivative of the magnification factor (see, e.g., S. A. Johnson et al. 2022; S. Sajadian 2023).

In Section 3.1, we offer an analytical relation for the peaks of overlapping self-lensing/occultation light curves and study the dependence of their values on relevant physical parameters. In Section 3.2, we evaluate the errors by using the offered analytical and approximate relations to estimate the peak values instead of their real values derived by the IRS method. We evaluate the widths of the self-lensing/occultation light curves as explained in Section 3.3.

3.1. Peaks of Light Curves: Estimation

In a self-lensing event and when the lens is over the source's disk and as far as $R_{\rm E} \ll R_{\star,\rm p}$, the image of the source star is a thick ring, where its inner and outer edges are $R_{\rm l} \simeq R_{\rm E}^2/R_{\star,\rm p}$ and $R_2 \simeq R_{\star,\rm p} + R_{\rm E}^2/R_{\star,\rm p}$. The inner radius is much smaller than the Einstein radius, and in most WDMS binary systems it is smaller than the WDs' radii. To show this point, maps of $\log_{10}[R_{\rm WD}/R_{\rm l}]$ over the 2D space $M_{\rm WD}(M_{\odot}) - \log_{10}[M_{\star}(M_{\odot})]$ are shown in the three top panels of Figure 4 by considering three orbital periods. Accordingly, only for long orbital periods $T \gtrsim 150$ days and when WDs are massive is $R_{\rm WD}$ less than $R_{\rm l}$, and the occultation does not change the light-curve peaks. In WDMS binary systems with low-mass WDs ($M_{\rm WD} \lesssim 0.2M_{\odot}$), the radii of the WDs are significantly higher than $R_{\rm l}$ (by 100 times or even more depending on the orbital period).

For an overlapping self-lensing/occultation signal, the peak in the stellar normalized flux can be given by

$$A_{\rm m} = A(\rho_{\star}, \Gamma) - \mathcal{O}(R_{\rm WD}, R_{\rm l}, R_{\star,\rm p}), \tag{6}$$

where $A(\rho_{\star}, \Gamma)$ is the maximum magnification factor. For a uniform source star, it can be estimated by $1 + 2\,\rho_{\star}^{-2}$. Also, $\mathcal{O} = \Theta(R_{\rm WD}^2 - R_{\rm l}^2)/R_{\star,\rm p}^2$ displays the occultation amount for a uniform source star and is the ratio of the image's area which is blocked by the lens to the source area. Here, Θ is a step function which is zero if $R_{\rm WD} \leqslant R_{\rm l}$. If $R_{\rm WD} > R_{\rm l}$, the value of the step function is $R_{\rm WD}^2 - R_{\rm l}^2$. The three middle panels of Figure 4 represent maps of $\mathcal{O}(\times 100)$ over the 2D space $M_{\rm WD}(M_{\odot}) - \log_{10}[M_{\star}(M_{\odot})]$ and for three values of the orbital period. If $R_{\star,\rm p} \gg R_{\rm E}$, one can find this analytical relation for $A_{\rm m}$ as follows:

$$\begin{aligned} A_{\rm m} &= 1 + \Delta A_{\rm m} \\ &\simeq 1 + \frac{2R_{\rm E}^2 - R_{\rm WD}^2}{R_{\star,\rm p}^2} + \frac{R_{\rm E}^4}{R_{\star,\rm p}^4} - 2\frac{R_{\rm E}^6}{R_{\star,\rm p}^6}. \end{aligned} \tag{7}$$

The higher terms, as far as $R_{\star,\rm p} \gg R_{\rm E}$, are much smaller and negligible. Similar approximate relations for the maximum deviation while self-lensing have been introduced before (E. Agol 2003; C. Han 2016). Here, we calculate its amount for different WDMS systems and discuss their properties. In real observations, the orbital period is uniquely determined because self-lensing and eclipsing signals are repeated with the period exactly equal to the orbital period. Hence, the masses of two companions (i.e., star and WD) are the free parameters that should be derived from the observed peak amount. We assume their radii are estimated using the known mass–radius relations (e.g., Equation (3)). We calculate $\Delta A_{\rm m} \times 100$ numerically and

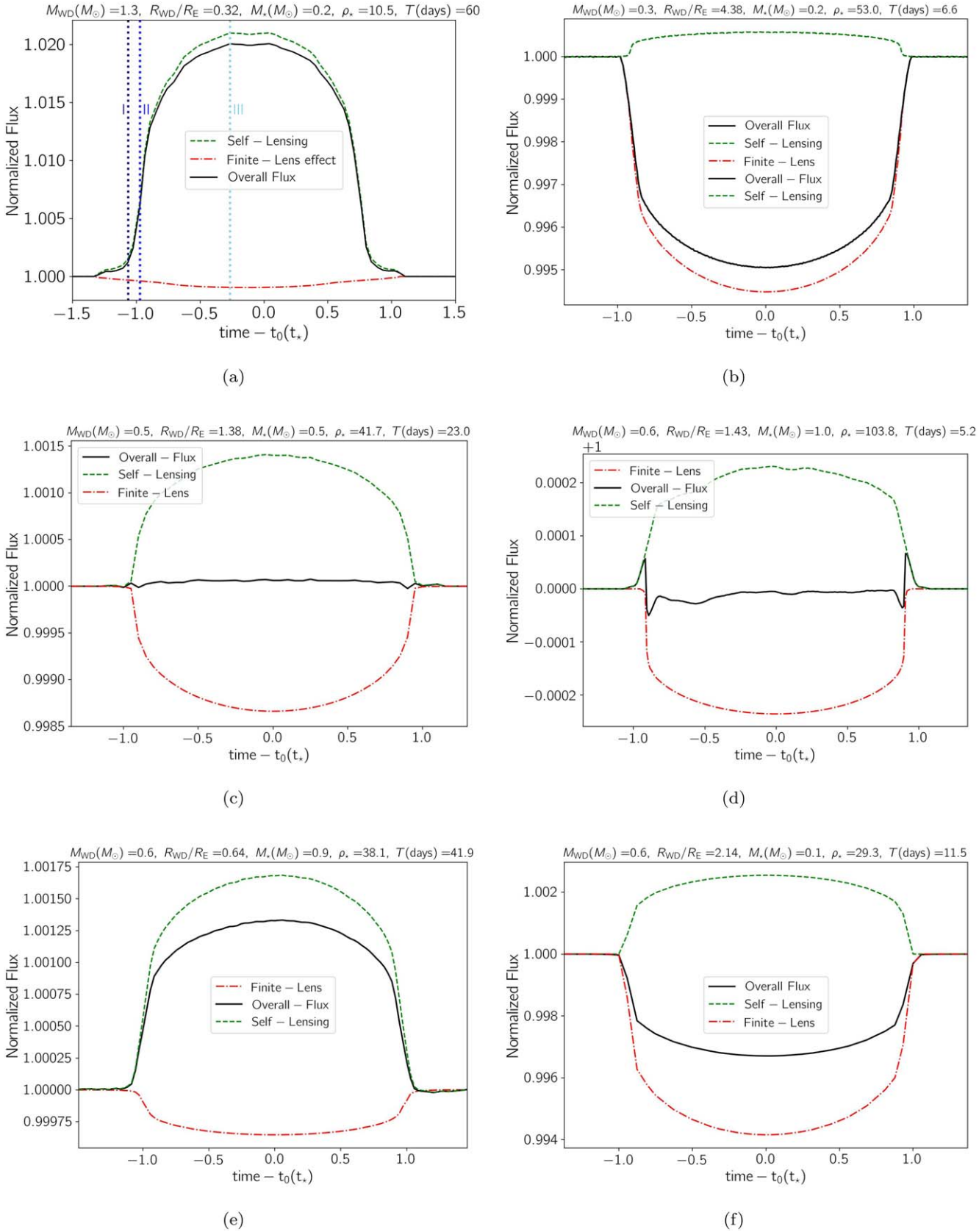

Figure 3. Examples of stellar light curves due to WDMS binary systems while the source stars are passing behind the compact objects. In these panels, self-lensing curves, obscuration curves due to finite-lens effects, and the overall light curves due to both self-lensing and finite-lens effects are shown by green dashed, red dotted–dashed, and black solid curves, respectively. The relevant parameters are given at the top of panels. The first panel shows the light curve due to the WDMS binary system whose lensing-induced images are represented in Figure 1.

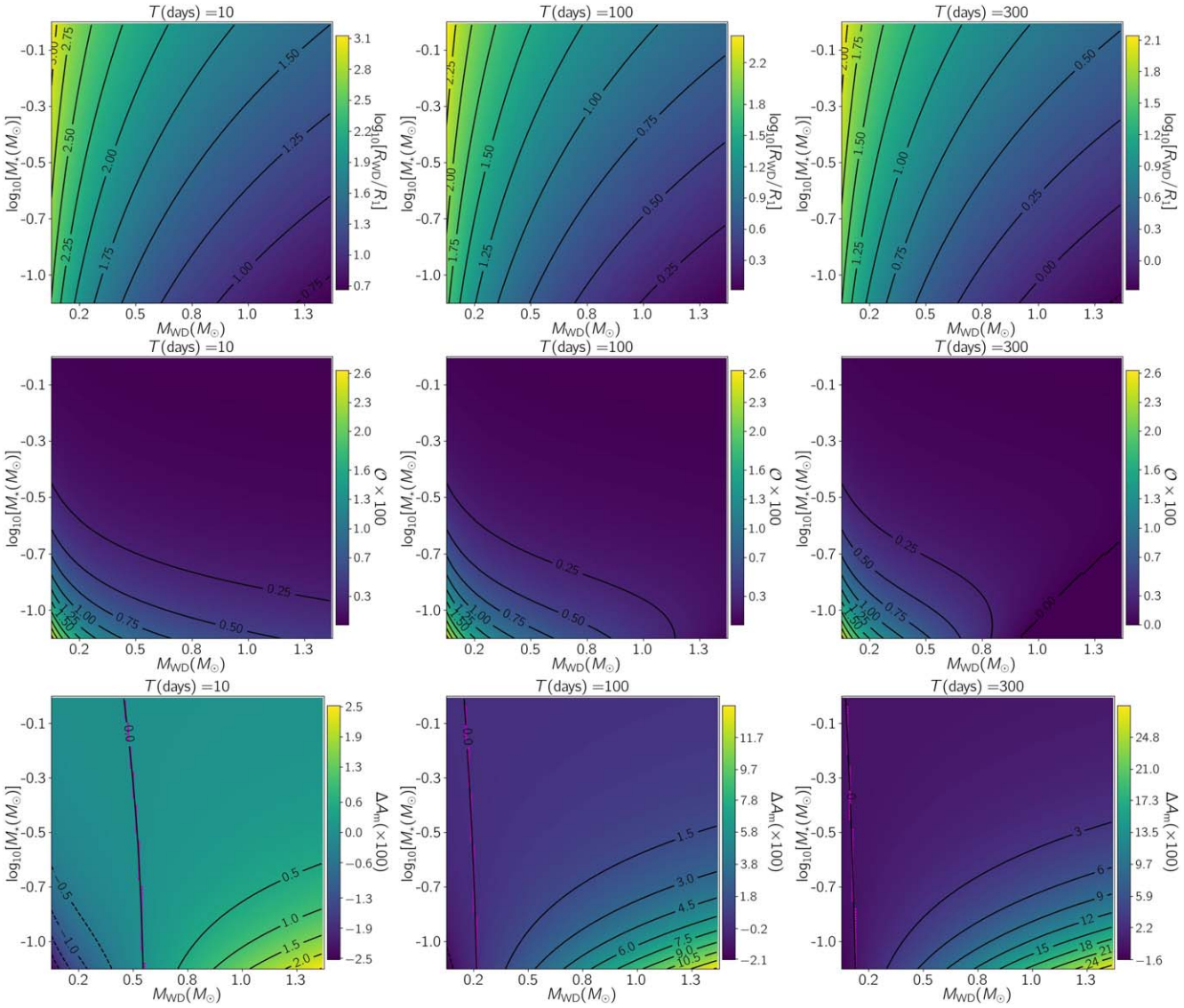

Figure 4. For three orbital periods $T = 10$, 100, and 300 days (from left to right), maps of $\log_{10}[R_{\rm WD}/R_{\odot}]$, $\mathcal{O} \times 100$, and $\Delta A_{\rm m} \times 100$ over the 2D space $M_{\rm WD}(M_{\odot}) - \log_{10}[M_{\star}(M_{\odot})]$ are displayed from top to bottom. The black curves show the contour lines for each map. Three animations from the maps of $\log_{10}[R_{\rm WD}/R_{\odot}]$ (https://iutbox.iut.ac.ir/index.php/s/gmxLytwMJWN84ni), $\mathcal{O} \times 100$ (https://iutbox.iut.ac.ir/index.php/s/QDJ8sfbbTdgiTKT), and $\Delta A_{\rm m} \times 100$ (https://iutbox.iut.ac.ir/index.php/s/tezLS7jKiHCzMiW) vs. orbital period are available.

display its maps over that 2D space in the three bottom panels of Figure 4. From these maps, the following points can be made:

1. Finite-lens effects are considerable when (i) the orbital period is short (some tens of days), and (ii) both the WD and its companion star are low-mass objects. We note that $R_{\rm WD}/R_{\odot}$ (or $R_{\rm WD}/R_{\rm E}$ as shown in the left panel of Figure 2) increases by $M_{\star}$. Nevertheless, the occultation effect on the stellar light curve, $\mathcal{O}$, decreases by $M_{\star}$, as it inversely depends on $R^2_{\star,\rm p}$.
2. The most massive WDs ($M_{\rm WD} \simeq 1.3 M_{\odot}$) produce large self-lensing signals which are dominant over their finite-lens effects even when considering wide ranges for the orbital period and the mass of companion stars. However, $\Delta A_{\rm m}$ increases when enhancing the orbital period.
3. Also, for a given WD and its companion star, $\Delta A_{\rm m}$ increases 3–5 times if their orbital period increases by 1 order of magnitude.
4. The contour line $\Delta A_{\rm m} = 0$ (which is highlighted with magenta color on the three bottom maps) shows that in their stellar light curves the WDMS binary systems' self-lensing and finite-lens effects cancel each other out. This contour line happens when $R_{\rm WD} \simeq \sqrt{2} R_{\rm E}$, where the main term in $\Delta A_{\rm m}$, as given by Equation (7), vanishes. These contour lines for each orbital period happen almost at a fixed $M_{\rm WD}$ and very weakly depend on $M_{\star}$. For instance, when $T = 10$, 100, and 300 days, $\Delta A_{\rm m} = 0$ when $M_{\rm WD}(M_{\odot}) \simeq 0.49$, 0.22, and 0.14. For a wide range of the orbital period, we numerically calculate $\overline{M_{\rm WD}}$ for which $\Delta A_{\rm m} = 0$, as shown in Figure 5 with a green dashed line. The lowest-mass WDs detected up to now have a mass of $0.17 M_{\odot}$ (see, e.g., M. Kilic et al. 2007; L. M. Calcaferro et al. 2018; W. R. Brown et al. 2020). This low limit on the WDs' mass is specified with a red dotted–dashed line in this figure. This line intersects with the line $R_{\rm WD} = \sqrt{2}\ R_{\rm E}$ at $T \simeq 200$ days. It means that in

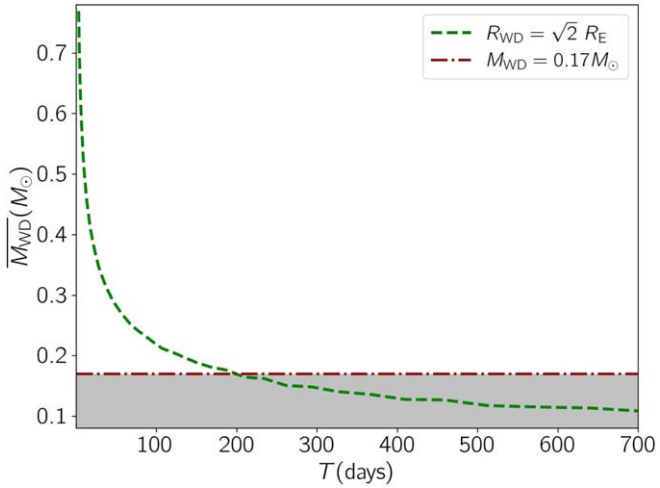

Figure 5. The average mass of WDs in WDMS binary systems for which $R_{WD} = \sqrt{2}\ R_E$ (where the self-lensing and occultation effects cancel each other out) vs. orbital period is plotted with a green dashed curve. The low limit on the WDs' mass specified is based on real observations (i.e., $0.17M_\odot$; see, e.g., M. Kilic et al. 2007; L. M. Calcaferro et al. 2018; W. R. Brown et al. 2020) and is represented with a red dotted–dashed line.

stellar light curves due to edge-on and wide WDMS binary systems with $T \gtrsim 200$ days, self-lensing and occultation signals do not cancel each other out completely.

5. The three bottom maps reveal the degeneracy while extracting M_{WD} and $M_\star$ from the maximum deviation in the normalized source flux during self-lensing/occultation ΔA_m. The contour curves show different values of M_{WD} and $M_\star$ that offer a given ΔA_m. However, the dependence (the variation rate) of ΔA_m on the WD mass is stronger than that of the mass of the companion star.
6. When the self-lensing signal dominates the finite-lens effect (i.e., $\Delta A_m > 0$) two parameters, M_{WD}, and $M_\star$, have reverse effects on ΔA_m so that either increasing the first one or decreasing the second enhances ΔA_m.
7. When the occultation due to the finite-lens effect dominates the self-lensing signal (i.e., $\Delta A_m < 0$), decreasing either M_{WD} or $M_\star$ increases the occultation's depth. Therefore, the masses of the WD and its companion star have the same effect on the occultation signals.
8. By considering the wide ranges for the WD and companion star masses ($M_{WD} \in [0.1,\ 1.4]M_\odot$ and $M_\star \in [0.08,\ 1.2]M_\odot$) and the orbital period ($T \in [3,\ 800]$ days) which are used to make maps/animations, we find the peaks of overlapping self-lensing/occultation light curves mostly occurs in the range $A_m \sim [0.975, 1.5]$.

3.2. Peaks of Light Curves: Error

E. Agol (2003) first offered an analytical solution for the magnification factor of a large source star by considering a limb-darkened profile for its brightness and the occultation effect due to the finite lens size. His analytical relation describes the peaks in self-lensing/occultation events well, as far as $\rho_\star \gg 1$. For that reason, in five discovered self-lensing events, modeling of light curves was done based on his formula. In most self-lensing events $\rho_\star$ is too large, except for WDMS binary systems with massive WDs in wide orbits (with long orbital periods).

Here, we evaluate the errors of using analytical relations while modeling self-lensing signals. We calculate peaks of overlapping self-lensing/occultation signals in different WDMS binary systems by considering a uniform stellar brightness two times, first using (i) the analytical relation given by Equation (6) (an approximate value) and then (ii) the IRS method (an accurate value $\Delta A_{m,IRS}$). Maps of their differences (Error $= \Delta A_m - \Delta A_{m,IRS}$) for three values of the orbital period are displayed in the top panels of Figure 6. According to these maps, to analyse the self-lensing/occultation signals when the companion stars are less massive and WDs are massive, using the approximate formula for the magnification (given by Equation (6)) could overestimate its peak up to 0.0018, 0.0082, and 0.0319 when the orbital period is $T = 30$, 100, and 300 days, respectively.

We note that these errors happen for WDMS binary systems including ultramassive WDs ($M_{WD} \gtrsim 1.2M_\odot$) and low-mass stars ($M_\star \lesssim 0.15M_\odot$). Substellar companions, even giant planets orbiting/transiting WDs, are common and can be detected through either eclipsing or infrared/near-infrared flux excess (see, e.g., J. Farihi et al. 2005; A. Vanderburg et al. 2020; A. Kosakowski et al. 2022; F. M. Jiménez-Esteban et al. 2023; T. Ferreira et al. 2024). Nevertheless, the mass distribution of WDs peaks at $\sim 0.6M_\odot$, with a low number of detected ultramassive WDs up to now (see, e.g., S. De Gennaro et al. 2008). Thus, the discussed errors in modeling self-lensing signals occur rarely, because ultramassive WDs are not common. The only detected substellar object around an ultramassive WD was reported recently by S. Cheng et al. (2024). They found one giant planetary companion for one of 3268 massive WDs reported in Gaia Data Release 3 (DR3; Gaia Collaboration et al. 2023).

Also, according to the top panels of Figure 6, this error will be higher for wider binary systems. Three discovered self-lensing events (whose Kepler IDs are KIC 03835482, KIC 06233093, and KIC 12254688) by H. Kawahara et al. (2018) have long orbital periods of $T \simeq 683$, 728, and 419 days, but their WDs and companion stars had masses of $M_{WD} \simeq 0.52$, 0.53, and $0.5M_\odot$ and $M_\star \simeq 1.3$, 1.1, and $1.4M_\odot$, respectively. Since their WDs' mass is half of solar mass, no significant errors occurred while modeling these events due to using analytical relations. Nevertheless, for these three targets we evaluated $\Delta A_{m,IRS}$, which resulted in Error $\simeq 4 \times 10^{-4}$, 5×10^{-4}, and 2×10^{-4}, respectively.

3.3. Widths of Light Curves

The overlapping self-lensing/occultation light curves shown in Figure 3 are similar to top-hat models, and their deviations from top-hat models are not large. Hence, we define their width as the time to cross the source disk by the lens object (which is somewhat different from the FWHM), as given by

$$\text{width} = 2t_\star, \quad t_\star = \frac{T}{2\pi}\left|\frac{\pi}{2} - \arccos\frac{R_{\star,p}}{a}\right|. \tag{8}$$

Here, we ignore the limb-darkening effect for the stellar brightness profile, while considering circular and completely edge-on orbits. As far as $R_{\star,p} \ll a$ for detached WDMS binary

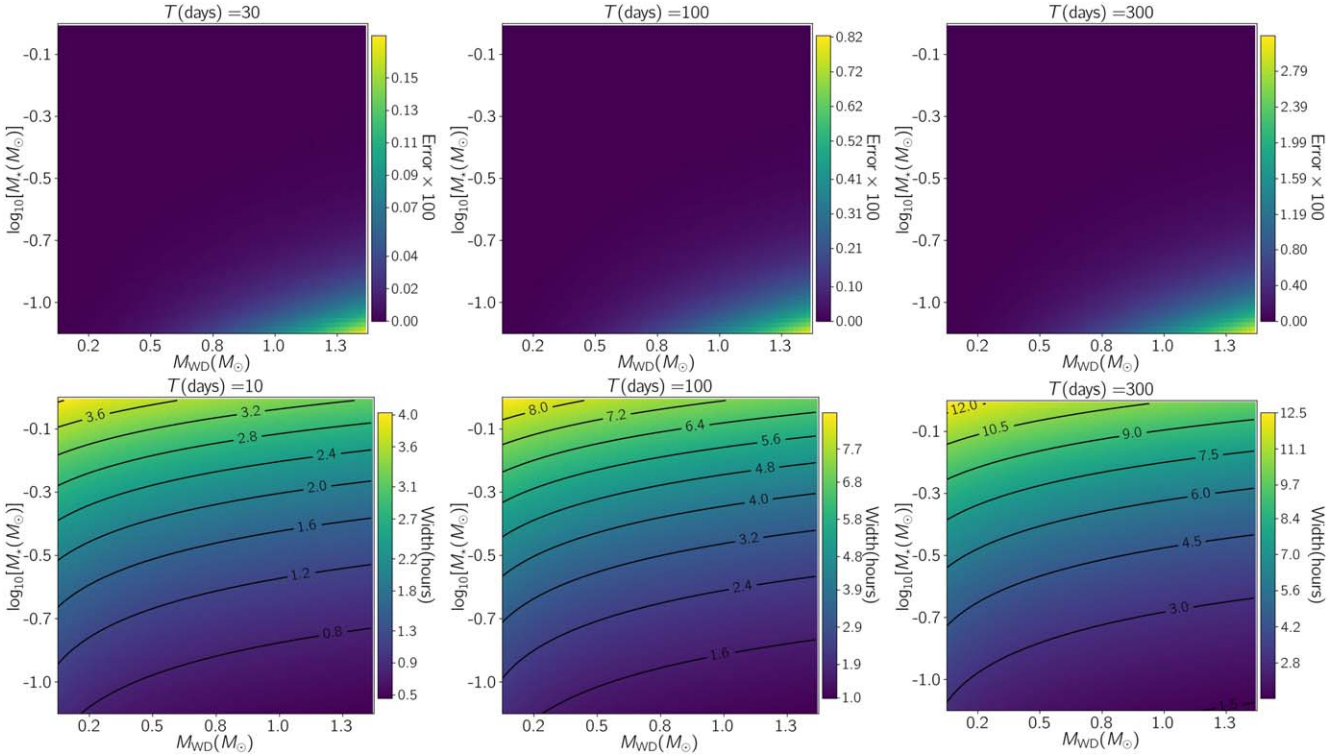

Figure 6. Top panels: maps of the overestimation of the maximum deviation in the normalized source flux while self-lensing ($\Delta A_{\rm m}$) owing to using Equation (7) as compared to their real values extracted by the IRS method. Bottom panels: maps of the width of the self-lensing/occultation light curves (given by Equation (8)) from different edge-on WDMS binary systems by considering three values for the orbital period. An animation (https://iutbox.iut.ac.ir/index.php/s/bb2fy7NEjwGEk2k) from the maps of light-curve width vs. orbital period is available.

systems, we can expand the arccos term, which results in

$$\text{width} \simeq \frac{T}{\pi}\left[\frac{R_{\star,\rm p}}{a} + \frac{1}{6}\left(\frac{R_{\star,\rm p}}{a}\right)^3 + ...\right]. \quad (9)$$

Accordingly, the width of a self-lensing/occultation signal is proportional to $\propto T^{1/3} R_{\star,\rm p}(M_\star + M_{\rm WD})^{-1/3}$. We estimate the widths of different stellar self-lensing/occultation light curves due to WDMS binary systems using Equation (8). Maps of these widths for three orbital periods and over 2D space $M_{\rm WD}(M_\odot) - \log_{10}[M_\star(M_\odot)]$ are represented in the three bottom panels of Figure 6. As mentioned, the light-curve width increases by $T^{1/3}$. For a given orbital period, smaller source stars make deeper self-lensing/occultation signals (see Equation (7)), but with smaller widths. Similarly, more massive WDs make deeper signals, but with smaller widths compared to less massive WDs.

To have a sense of the widths of the possible self-lensing/occultation light curves for different orbital periods, in Figure 7 we show the range of all possible width values (dotted–dashed black curves) and their average (dashed black curve) versus the orbital period as specified on the left vertical axis. If we assume that in order to discern any self-lensing/occultation signal at least five data points should be recorded, the worst cadence to capture the signals with a given orbital period is $\text{Cadence}_{\rm max}(\text{minute}) = \text{Maximum}(T) \times 12$, which is shown in this figure with a magenta solid line and specified on the right vertical axis. Accordingly, any survey observations with a cadence worse than 110, 50, and 30 minutes could not find any self-lensing/occultation signals due to WDMS binary systems with orbital periods less than ∼100, 10, and 3 days,

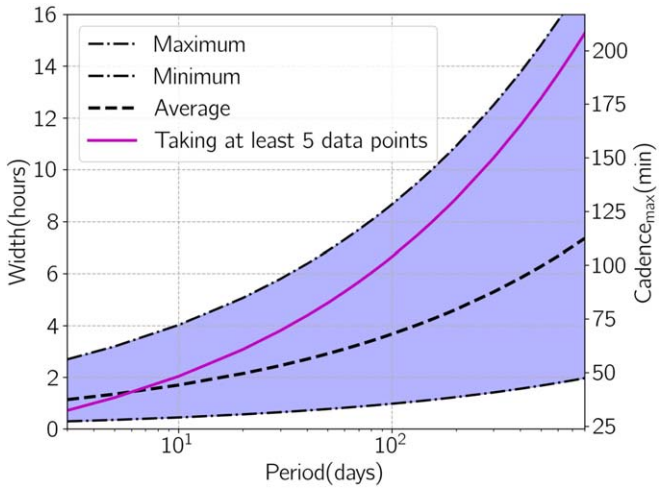

Figure 7. The ranges and the average of possible widths (specified on the left vertical axis) due to different self-lensing/occultation signals from different WDMS binary systems are shown with dotted–dashed and dashed black curves vs. the orbital period, respectively. We assume at least five data points should cover signals so that they can be realized. In that case, the worst cadence vs. the orbital period for realizing these self-lensing/occultation signals is $\text{Cadence}_{\rm max}(\text{minute}) = \text{Maximum} \times 12$ and is plotted with a magenta solid line as specified on the right vertical axis.

respectively. To evaluate the light-curve width in Equation (8), we assumed (i) the inclination angle is zero, (ii) the stellar brightness is uniform without any limb-darkening effect, and (iii) the stellar orbit around the compact object is circular with a constant speed. The first two simplifications lead to an overestimation for the light-curve width. Hence, with the determined $\text{Cadence}_{\rm max}$ we may miss some short self-lensing/

eclipsing signals due to a limb-darkened source star and higher inclination angle.

4. Conclusions

In this work, we studied the finite-lens effect in self-lensing signals due to edge-on and detached WDMS binary systems analytically (based on a close approximation to reality) and numerically (using the IRS method). The finite-lens effect refers to the obscuration of some part of the image's area by the lens's disk. In WDMS binary systems with orbital radii around 1 au, their Einstein radii are ~ 0.02–$0.05 R_{\odot}$, which is the same order of magnitude as the radius of a common WD. Hence, during self-lensing due to WDMS binary systems, the compact object can block some parts of the image's disk which are inside the Einstein ring.

To find in what WDMS systems this occultation effect is considerable, we first calculated $R_{\rm WD}/R_{\rm E}$ for different masses of WDs and source stars versus the orbital period. We concluded that for most WDs and source stars with $M_{\rm WD} \gtrsim 0.2 M_{\odot}$, and $M_{\star} \in [0.08, 1.2] M_{\odot}$, if their orbital periods are $T \gtrsim 300$ days, the magnification due to self-lensing dominates over the occultation owing to the finite-lens effect. For most massive WDs with $M_{\rm WD} \gtrsim 1.3 M_{\odot}$ with very small radii, even considering a wide range for the orbital period $T \in [5,\ 1000]$ days and different values for $M_{\star}$, we do not expect a significant finite-lens effect, since for them $R_{\rm WD} \lesssim 0.6 R_{\rm E}$.

Generally, self-lensing signals dominate finite-lens effects when $R_{\rm E}$ is large. The highest self-lensing signal happens for most massive WDs ($M_{\rm WD} \sim 1.3 M_{\odot}$) that have dwarf companions in wide orbits. Inversely, occultation dominates over the self-lensing signal when $R_{\rm E}$ is small, e.g., for WDMS systems with low-mass WDs ($M_{\rm WD} \sim 0.2 M_{\odot}$) and dwarf companion stars in close orbits with short orbital periods $T \lesssim 50$ days. We noted that both effects (i.e., magnification and occultation) are enhanced when the source radius is reduced. Also, for long orbital periods $T \gtrsim 150$ days and when WDs are massive, there is no occultation effect.

We also confirmed these results by evaluating the occultation amounts, $\mathcal{O}$, and the maximum deviations in the stellar normalized flux (due to overlapping self-lensing and occultation effects) for different WDMS binary systems, $\Delta A_{\rm m}$, based on the analytical and approximate relations. Considering the wide ranges of WD and companion star masses and orbital periods that are applied in the making of maps/animations, the peaks of the self-lensing/occultation light curves mostly occur in the range $\Delta A_{\rm m} \in [0.975, 1.5]$.

Using the IRS method, we made stellar light curves for detached and edge-on WDMS binary systems and when the source star passes behind the compact object. In these light curves, self-lensing and occultation due to the finite lens size canceled each other out when $R_{\rm WD} \simeq \sqrt{2} R_{\rm E}$, regardless of the source radius. This condition happens for a certain $M_{\rm WD}$ for any given value of the orbital period. For instance, self-lensing and occultation cancel each other out when $M_{\rm WD}(M_{\odot}) \sim 0.49$, 0.22, and 0.14 when the orbital period is $T = 10$, 100, and 300 days, respectively. Considering the fact that the lowest-mass WDs detected up to now have a mass of $0.17 M_{\odot}$ (M. Kilic et al. 2007; L. M. Calcaferro et al. 2018; W. R. Brown et al. 2020), for the WDMS binary systems with $T \gtrsim 200$ days the cancellation of self-lensing and occultation signals never happens.

Because all five self-lensing events discovered up to now (E. Kruse & E. Agol 2014; H. Kawahara et al. 2018; K. Masuda et al. 2019; N. Yamaguchi et al. 2024) were modeled using the known analytical and approximate relation (given in Equation (7)), we evaluated the values of overestimation in $\Delta A_{\rm m}$ with respect to the real amounts extracted by the IRS method by using the analytical relation. Maps of these deviations are given in the three top panels of Figure 6 for three given values of the orbital period. According to these maps, analyzing the self-lensing signals using the approximate formula for the magnification could overestimate its peak up to 0.0018, 0.082, and 0.0319 when the orbital period is $T = 30$, 100, and 300 days, respectively. These maximum overestimations occur for WDMS systems including ultramassive WDs ($M_{\rm WD} \gtrsim 1.2 M_{\odot}$) and substellar companions ($M_{\star} \lesssim 0.15 M_{\odot}$). None of those five discovered self-lensing events were such systems. Generally, the number of detected ultramassive WDs is rare.

Finally, we studied the dependence of the stellar light-curve width on the physical parameters, which is width $\propto R_{\star,\rm p}\, T^{1/3} (M_{\star} + M_{\rm WD})^{-1/3}$. Accordingly, smaller source stars make deeper signals, but with shorter durations in comparison to larger ones. We considered a wide range of masses for the WDs and MS source stars in completely edge-on orbits and with a uniform brightness for stellar disks, and estimated the widths of their light curves. Based on these assumptions, we concluded any survey observations with a cadence worse than 110, 50, and 30 minutes will not find any self-lensing/occultation signals due to WDMS binary systems with an orbital period of less than 100, 10, and 3 days, respectively. However, even with better cadences some signals due to more inclined systems and limb-darkened source stars may be missed.

Acknowledgments

The authors thank the anonymous referee for their careful and useful comments.

All simulations that have been done for this paper are available online (http://github.com/SSajadian54/FiniteLensEffect). Also, the codes, animations, figures, and several examples of generated light curves can be found in a Zenodo repository (S. Sajadian 2024).

ORCID iDs

Sedighe Sajadian https://orcid.org/0000-0002-2859-1071
Hossein Fatheddin https://orcid.org/0000-0002-7611-9249

References

Agol, E. 2002, ApJ, 579, 430
Agol, E. 2003, ApJ, 594, 449
Ambrosino, F. 2020, arXiv:2012.01242
Brown, W. R., Kilic, M., Kosakowski, A., et al. 2020, ApJ, 889, 49
Calcaferro, L. M., Althaus, L. G., & Córsico, A. H. 2018, A&A, 614, A49
Cheng, S., Schlaufman, K. C., & Caiazzo, I. 2024, arXiv:2408.03985
Clark, E. E. 1972, MNRAS, 158, 233
De Gennaro, S., von Hippel, T., Winget, D. E., et al. 2008, AJ, 135, 1
Dominik, M. 1998, A&A, 329, 361
Einstein, A. 1936, Sci, 84, 506
Farihi, J., Becklin, E. E., & Zuckerman, B. 2005, ApJS, 161, 394
Ferreira, T., Saito, R. K., Minniti, D., et al. 2024, MNRAS, 527, 10737
Gaia Collaboration, Vallenari, A., Brown, A. G. A., et al. 2023, A&A, 674, A1
Gaudi, B. S. 2012, ARA&A, 50, 411
Gould, A. 1995, ApJ, 446, 541
Gould, A., & Gaucherel, C. 1996, arXiv:astro-ph/9606105

Han, C. 2016, ApJ, 820, 53
Jiménez-Esteban, F. M., Torres, S., Rebassa-Mansergas, A., et al. 2023, MNRAS, 518, 5106
Johnson, S. A., Penny, M. T., & Gaudi, B. S. 2022, ApJ, 927, 63
Kawahara, H., Masuda, K., MacLeod, M., et al. 2018, AJ, 155, 144
Kayser, R., Refsdal, S., & Stabell, R. 1986, A&A, 166, 36
Kilic, M., Allende Prieto, C., Brown, W. R., & Koester, D. 2007, ApJ, 660, 1451
Kosakowski, A., Kilic, M., Brown, W. R., Bergeron, P., & Kupfer, T. 2022, MNRAS, 516, 720
Kruse, E., & Agol, E. 2014, Sci, 344, 275
Liebes, S. 1964, PhRv, 133, B835
Maeder, A. 1973, A&A, 26, 215
Masuda, K., Kawahara, H., Latham, D. W., et al. 2019, ApJL, 881, L3
Narayan, R., & Bartelmann, M. 1996, arXiv:astro-ph/9606001
Refsdal, S., & Bondi, H. 1964, MNRAS, 128, 295
Renn, J., Sauer, T., & Stachel, J. 1997, Sci, 275, 184
Ricker, G. R., Winn, J. N., Vanderspek, R., et al. 2014, Proc. SPIE, 9143, 914320
Riess, A. G., Anand, G. S., Yuan, W., et al. 2024, ApJL, 962, L17
Riess, A. G., Filippenko, A. V., Challis, P., et al. 1998, AJ, 116, 1009
Sahu, K. C., Anderson, J., Casertano, S., et al. 2022, ApJ, 933, 83
Sajadian, S. 2021, MNRAS, 506, 3615
Sajadian, S. 2023, MNRAS, 521, 6383
Sajadian, S. 2024, Finite-lens Effect on Self-lensing in Detached White Dwarfs-main Sequence Binary Systems, Zenodo, doi:10.5281/zenodo.13851505
Sajadian, S., & Afshordi, N. 2024, arXiv:2409.12441
Sajadian, S., & Hundertmark, M. 2017, ApJ, 838, 157
Sajadian, S., & Rahvar, S. 2010, MNRAS, 407, 373
Schneider, P., Ehlers, J., & Falco, E. E. 1992, Gravitational Lenses (Berlin: Springer)
Schneider, P., & Weiss, A. 1987, A&A, 171, 49
Soldner, J. 1921, AnPhy, 370, 593
Sorabella, N. M., Laycock, S. G. T., Christodoulou, D. M., & Bhattacharya, S. 2024, ApJL, 961, L45
Vanderburg, A., Rappaport, S. A., Xu, S., et al. 2020, Natur, 585, 363
Wambsganss, J. 1998, LRR, 1, 12
Witt, H. J., & Mao, S. 1994, ApJ, 430, 505
Yamaguchi, N., El-Badry, K., Ciardi, D. R., et al. 2024, PASP, 136, 074201